Impact of relative humidity on the mechanical behavior of compacted earth as a building material

Champiré, F. , Fabbri, A. , Morel, J. C. , Wong, H. and McGregor, F.

Original citation & hyperlink:
Champiré, F. , Fabbri, A. , Morel, J. C. , Wong, H. and McGregor, F. (2016) Impact of relative humidity on the mechanical behavior of compacted earth as a building Material. *Construction and Building Materials*, volume 110 : 70-78
http://dx.doi.org/10.1016/j.conbuildmat.2016.01.027

DOI 10.1016/j.conbuildmat.2016.01.027
ISSN 0950-0618

Publisher: Elsevier

Impact of relative humidity on mechanical behavior of compacted earth for building constructions

Florian Champiré[1], Antonin Fabbri[1] *, Jean-Claude Morel[2], Henry Wong[1], Fionn McGregor[1]

[1]*LGCB-LTDS, UMR 5513 CNRS, ENTPE, Université de Lyon, 69100 Vaulx-en-Velin, France ;*

[2]*School of Energy, Construction and Environment, Faculty of Engineering, Environment and Computing, Coventry University ;*

*Corresponding author: Tel. :+33-472-047-286 ; Fax : +33-472-047-156 ; email : antonin.fabbri@entpe.fr

1. Abstract

Earthen buildings can provide an answer to facing difficulties in modern constructions in both terms of sociology, economics and ecology. However, the difficulty to understand and to predict their long term behavior represents an obstacle to their spreading as, for example, unsuitable interventions on old constructions which are leading to catastrophic situations.

To be more specific, during their lifetime, the earthen walls have to face important variations of indoor and outdoor relative humidity, which induce variations and gradients in their water content. In this context, this paper aims at addressing an important aspect, not yet fully understood: the impact of these variations on the deformability (axial, volumetric) and the strength of unstabilized earth. To that purpose, unconfined compression tests, with and without unload-reload cycles, were performed on different earthen material samples conditioned at different relative humidity. Tested samples were made out of materials coming from different existing constructions and sieved at 10 mm. During the tests, the axial and radial deformations were measured through non-contact sensors and an image correlation system. This study allows underlining a complex volumetric behavior, as well as plastic and damage phenomena, which both show a strong dependence on the relative humidity at which the samples were stored, but also on the activity of the clayey content of the earth.

Keywords: Earth material, compacted earth blocks, relative humidity, water content, compressive strength, stress-strain behavior, volumetric behavior.

2. Introduction

A recent growing interest in earthen constructions in occidental countries is observable, mostly due to their low environmental impact [1]. Indeed, earthen material needs few or no transformation to be used as a construction material and is extracted close to the construction site. Moreover, the wall thickness, ranging from 30cm to 50cm, and the affinity of raw earth for water molecules bring a well-known quality for interior comfort at both acoustic, hygric and thermic levels [2]–[5]. The water in the wall plays a crucial part: it confers a cohesion of the material, through suction effects, and is also able to buffer temperature variations through liquid/vapor phase change phenomena, thus increasing the apparent thermal inertia of the wall [2]–[5]. However, the development of this ancestral building technique notably suffers from the lack of appropriate standards for construction and restoration, dealing accurately with mechanical, hydraulic, and even mineralogical characteristics of the earthen materials as well as their couplings, not yet fully understood.

To fill this gap, many laboratory tests have been made on earth samples and walls [6]–[8]. These studies underline an important variability of the common parameters such as the compression strength and the Young's modulus, which depend on the sample geometry, earths used and test conditions. In addition, the knowledge of only these two parameters are found to be insufficient to properly model the complex behavior of earthen walls [9]–[11]. For example, assumptions considering a Poisson's ratio equal to 0.33 (i.e. like a soil material [12]), and elastic moduli independent of the water content are known to be inconsistent with experimental observations [13]. Furthermore, the material strength is usually evaluated through the compressive strength using unconfined compression tests and sometimes through the tensile strength using splitting or three points bending tests [14]. Measuring these parameters with no temperature nor relative humidity regulation is suitable for conventional materials such as concrete and stone. However, when it comes to the earth behavior and knowing its strong interaction with water molecules, it will be interesting and necessary to check the impact of ambient temperature and relative humidity [15]. As already discussed by many authors, the inherent variability of earth types and the influence on its behavior of hygrothermal external conditions, make the identification of the key parameters (i.e. whose determination should be sufficient to qualify the mechanical performance of the material) even more difficult.

In this context, this paper aims at quantitatively studying the mechanical behavior of different unstabilized earths used for building constructions, and more precisely, at identifying main global trends, each of them

investigated considering the impact of the relative humidity. It is a preliminary but essential step towards the development of a well-adapted constitutive model.

For that purpose, unconfined compression tests with and without unload-reload cycles and at different relative humidity were performed. The tested samples were made of earth sieved at 10mm and coming from three existing rammed earth constructions. During the test, the axial and radial strains were measured using non-contact sensors and an image correlation system so that the elastic parameters (namely Young's modulus and Poisson's ratio), the unconfined compressive strength, the residual strains and the volume variations can be measured with accuracy for every test conditions.

There are different building techniques using clayey material: rammed earth, adobe, cob, earth masonry, Compacted Earth Blocks (CEB), Extruded Earth Blocks, wattle and daub [16]. The choice is mostly made on the local know-how and on the nature of the soil. In any case, the material is composed of aggregates (sand, gravels, fibers, etc…) bonded by a continuous clayey matrix, which is known to be responsible for the cohesion of the material and its complex mechanical behavior, such as swelling and shrinkage when subjected to hydric changes [17], [18]. As a consequence, even though studied materials are CEB, the conclusions can be, up to a certain point and given an equivalent clay mass content, extended to other earthen construction technics. At last, many tests found in the literature study the impact of stabilizers (i.e. adding a binder, concrete or lime) on the mechanical behavior of the material [19]–[23], which are shown to be often responsible for an increase of the compression strength and a reduction of the impact of water on the mechanical behavior. If the existence of environmental side-effects has to be mentioned [15], [24], [25], the use of stabilizers has proven to be necessary for environmental (monsoon, etc…) or specific structural constraints. However, the heritage of unstabilized earth buildings remains particularly important [11], and must be assessed, at least for maintenance and rehabilitation purposes. That is the reason why this study was limited to the behavior of the compacted earth without stabilizer (i.e. only composed by crude clayey soils).

The first part of the paper describes the earthen materials tested, the sample preparation and the experimental procedures. The results of the unconfined compression tests are presented in the second part. Finally, the last paragraphs focus on the most important factors governing the mechanical behavior: type of soil, relative humidity and the maximum applied stress.

3. Materials and methods

3.1. Material

Three different materials were studied, named STR, CRA and ALX. They all came from existing centenarian rammed earth constructions located in "Rhône-Alpes" region in the South-East of France, thus ensuring that the studied material was suitable for building sustainable earth constructions [26]. The particle size distributions of all three earths were determined with the French Norms NF P94-056 and NF P94-057 and are reported in Figure A and they lead to a mass content of clays (particles with a diameter lower than 2µm) equal to 15% for STR, 16% for CRA and 8% for ALX.

In parallel, the Atterberg limits and the Methylene Blue Value (MB) are made of the 0-80µm proportion of the soils. The choice has been made in order to increase the accuracy of the measurement and to provide a direct comparison between the activities of the fine components (clays + silts) of the tested materials. The measurement of the activity was made following [27]. Finally, the clay minerals were identified using a Siemens D5000 powder X-ray diffractometer equipped with a monochromator having a Ka (lambda = 1.789 Å) cobalt anticathode on oriented aggregates and using three preparations: air dried or natural, after glycolation and after heat treatment at 500 °C. The clay characteristics are summarized in Table 1.

Table 1: Characteristics of the 0-80µm fraction of the three selected earths.

	STR	**CRA**	**ALX**
Liquid limit **(W_l)**	24%	29%	20%
Plastic limit **(W_p)**	18%	16%	16%
Plasticity index **(I_p)**	7%	14%	4%
Blue value **(MB)**	1.0	2.7	0.8
Main clay minerals	Illite+Chlorite	Illite+Kaolinite	Illite+Vermiculite

The RXD analysis shows that the clays of the three materials are quite stables (illite, Kaolinite, Chlorite and Vermiculite). These results are quite consistent with the common know-how which stipulate that the clay content proportion should thus be sufficient to ensure a good material stiffness and strength, but the proportion of expansive clay must remain limited in order to avoid cracking.

The plasticity index and the Methylene Blue Value of the 0-80µm proportion of CRA are at least twice as high as STR's ones, while their particle size distributions are similar. On the other side, Methylene Blue Value of the 0-80µm proportion of STR and ALX are similar.

Finally, a non-prescriptive recommendation, suggested by [28] and named BS1377-2:1990, provides a criterion to identify suitable soils for rammed earth constructions based on the shape of the particle size distribution. However, none of the three studied particle size distributions fit within the given area, despite the fact that these soils were from existing constructions. As a consequence, the particle size distribution alone does not appear to be sufficient to decide whether or not a given type of earth is suitable for rammed earth constructions. This fact has already been mentioned by [28] and [29] for rammed earth but also for adobe constructions.

Sorption isotherms, measured for each material at 24°C according to the standard NF EN ISO 12571:2000, are presented in Figure B. These curves characterize the water intake with increasing ambient humidity and at constant temperature. The desorption isotherms, characterizing water expulsion with decreasing ambient relative humidity at constant temperature, are not studied in this paper.

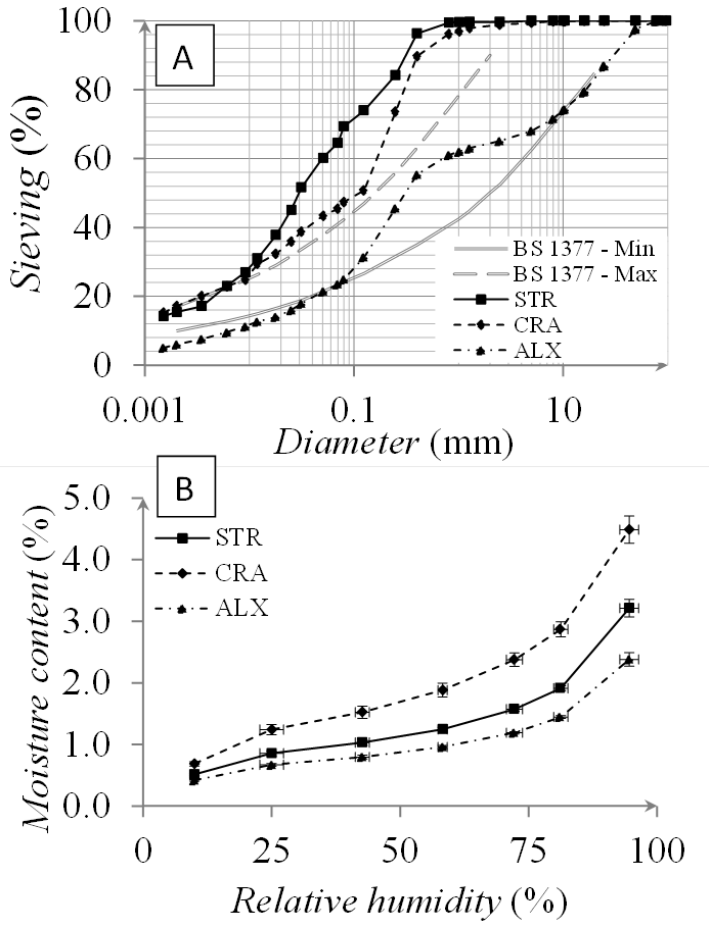

Figure 1: Particle size distributions of the tested materials and their comparison with the upper and lower bounds of the BS 1377 Standard (A) and their sorption curves (B)

In Figure B, it can be seen that the moisture content of the CRA-earth is the highest for each given relative humidity. This observation is consistent with the MB value of the 0-80µm proportion of the materials. Indeed,

adsorption capacity is known to increase with the cation exchange capacity [30], which is, in turn, linked to the MB value

3.2. Samples preparation

The earth blocks samples from the rammed earth buildings were crushed and dried at ambient relative humidity and temperature. The earth was sieved at 10mm, moisturized up to the target moisture content and mixed in a blender. The sieving stage was not realized on STR and CRA since their biggest particles are smaller than 10mm. It means that all the laboratory tests are representative of the on-site material for these two earths.

The compacted earth blocks (CEB) are manufactured according to [31] with a double compaction manual press. In particular, to determine of the optimum moisture content, CEBs at 5 water content (7%, 9%, 11%, 13% and 15%) and with different material quantities (from 8.6 to 9.2kg with an increasing step of 0.2kg) are prepared. Among them, the "optimum" couple of water content / earth quantity is the one which gives the highest bulk density. These optimum values for each earths are reported in Table 2. In the following of the paper, all the tested materials are manufactured at their optimum moisture content and earth quantity.

Table 2 : Characteristics of the Compacted Earth Blocks

Earth	Optimum moisture content (%)	Fabrication weight (kg)	Bulk density (g/cm^3)	Porosity (%)
ALX	9%	9.0	1.98	25%
CRA	11%	8.8	1.97	26%
STR	11%	8.8	1.95	26%

Many published works show the importance of the sample shapes and the nature of its interfaces with the press [7], [12], [32], [33]. In [12], cylindrical samples exhibit a lower compressive stress than prismatic ones. However, the comparison of these results is not so easy because the contact areas between the sample and the press are not the same. Nevertheless, Hall and Djerbib [7] recommend the use of a pondering coefficient to reduce the compressive strength on prismatic samples to fit measurements on cylindrical samples. Cylindrical samples were thus chosen for the following study. Regarding the interface, there is no consensus on the benefits of adding a rubber or a piece of wood between the sample and the press. Indeed, according to [12], [32], such interface can improve the repeatability of the tests, but [19] highlights the occurrence of localized damage next to the interfaces. Anyway, the impact of this additional interface becomes negligible when the

aspect ratio (i.e. length divided by diameter) of the samples is higher than or equal to 2. Consequently, given an aspect ratio superior to 2, the compression tests were carried out without interface components on cylindrical samples.

These samples were cored within the CEB, perpendicularly to its lateral surface, across its width and with no additional water. The samples finally had a diameter of 64.4 mm and a length of 140 mm, with an aspect ratio of 2.17. Before the coring, the CEBs were dried at 50°C to increase their consistency. This step is necessary to avoid disturbance on the sample surfaces. Before samples conditioning and in order to use correlation system, which is explained in the next section, samples were flecked with black spray.

To assure a controlled relative humidity, the samples were conditioned in home-designed hermetic boxes, themselves stored in a climatic chamber at a constant temperature of 24°C ± 2°C. The relative humidity inside the boxes was regulated with saline solutions according to the NF EN ISO 12571:2000 standard, and was homogenized thanks to a micro-fan. The temperature and relative humidity were controlled with HMP50 sensors from Campbell Scientific, Inc., Logan, UT. The samples were regularly weighted twice a day to check the water intake. Once the equilibrium is reached (i.e. constant mass with a variation lower than 2% for at least one week), the sample were tested.

The compression tests were not performed in a humidity-controlled environment and lasted nearly thirty minutes. Consequently, it was necessary to check the evolution of the water content of the material. However, since the samples were tested until failure, it was not possible to control directly their water loss or gain from the beginning to the end of the test. To do so, the mass variation of reference samples was measured, conditioned at the same relative humidity and placed in the same conditions as during a real test (i.e. with lights and sensors). The most significant relative mass variation was about 5%, obtained for the earth STR stored at 97%RH. According to the sorption isotherms reported in Figure B, this leads to a maximum uncertainty of about 2% in relative humidity, which is acceptable.

3.3. Experimental set-up

The unconfined compression tests were performed with the electro-mechanical press (Z020TN, Zwick Roell, Ulm, Germany). The accuracy of the sensors was about 20 N for the strength and 0.018 µm for the displacement.

The axial strains were measured using an image correlation method, with two pairs of cameras (System 1 and System 2), enabling the acquisition of two pictures per second each. As presented schematically in Figure 2, the angle between each pair of cameras was equal to 120°, while the angle between the two cameras of the same pair (top and bottom) was 32°. The distance between the camera and the sample was 35 cm. This layout enables a theoretical accuracy of 0.8 µm along the displacement axis. Optical system characteristics is given in Table 3.

Table 3: Optical system characteristics

Camera	
Label	Allied vision technologies
Model	Pike F-421B/C
Resolution	4.2 MPixel
Width pixel	7.4 µm

Lens	
Label	Schneider
Model	2.0/28-0901
Focal distance	28mm
Opening diaphragm	16

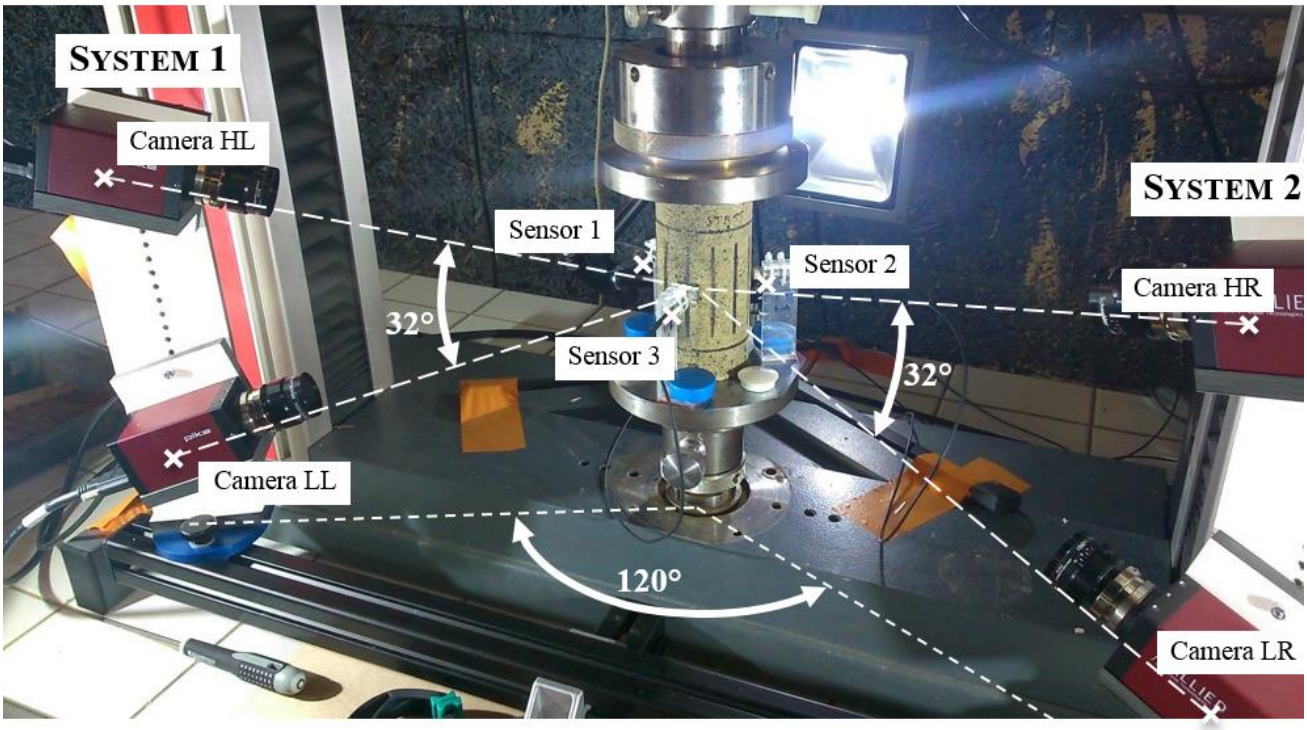

Figure 2 : Geometric arrangement of the cameras

It was necessary to use a lens with a small diaphragm opening (16) to improve depth of field as the surface to be observed is cylindrical. This small opening thus requires a powerful spot light and an exposure time of about 80ms.

185 The sample surfaces were flecked with black paint spray to create speckles. The image correlation method is
186 performed by the commercial software Vic-3D (Correlated Solutions). The software uses “subsets” which are
187 identical squares gathering from 10 to 20 speckles (see Figure 3) and follows the displacement of their center
188 and the deformation around it from an image to another. The speckles have to be as small as possible but, at
189 the same time, big enough to be detected by the camera (i.e. higher than 25µm, which corresponds to 3
190 pixels). Indeed, the smaller the speckles (and thus the subsets) are, the more accurate the displacement and
191 deformation calculation will be [34].

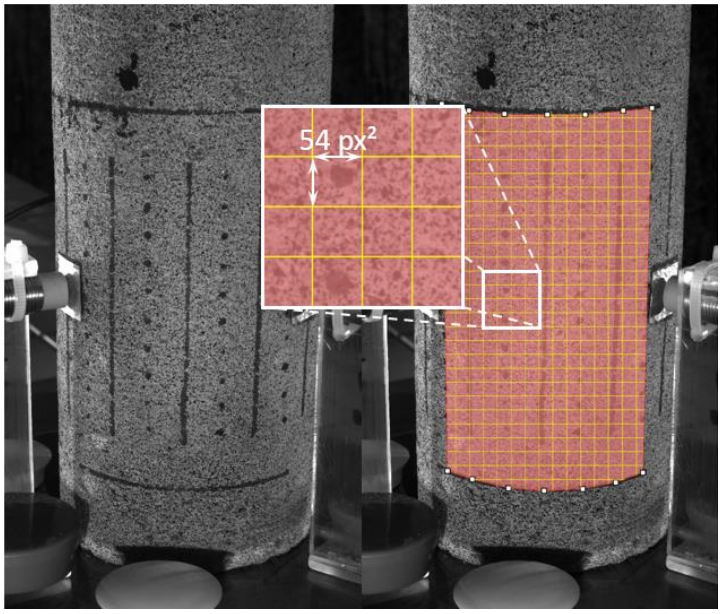

192
193 Figure 3: Sample speckled at left and the his grid defined by Vic-3DR at right

194 The subsets size can be set manually or be defined by the software. As a consequence, it can be interesting to
195 study the impact of the subsets size on the deformation calculation. Three sizes were chosen: 26 px^2, 54 px^2
196 (determined by the software) and 108 px^2 (px=pixel). The main aspect of the axial deformation was similar
197 from a case to another (some deformation fields being more accurate than others).

198 As shown in Figure 4, the displacement was calculated along the vertical axis (z) leading to the colored
199 surface. The two pairs of cameras (called systems 1 and system 2) are represented. The image correlation
200 device provided the displacement field on the two-thirds of the sample surface all throughout the test. Two
201 points, forming a numerical extensometer, were placed to measure the sample deformation. The average axial
202 deformation is calculated from the average of the four numerical extensometers represented in Figure 4.

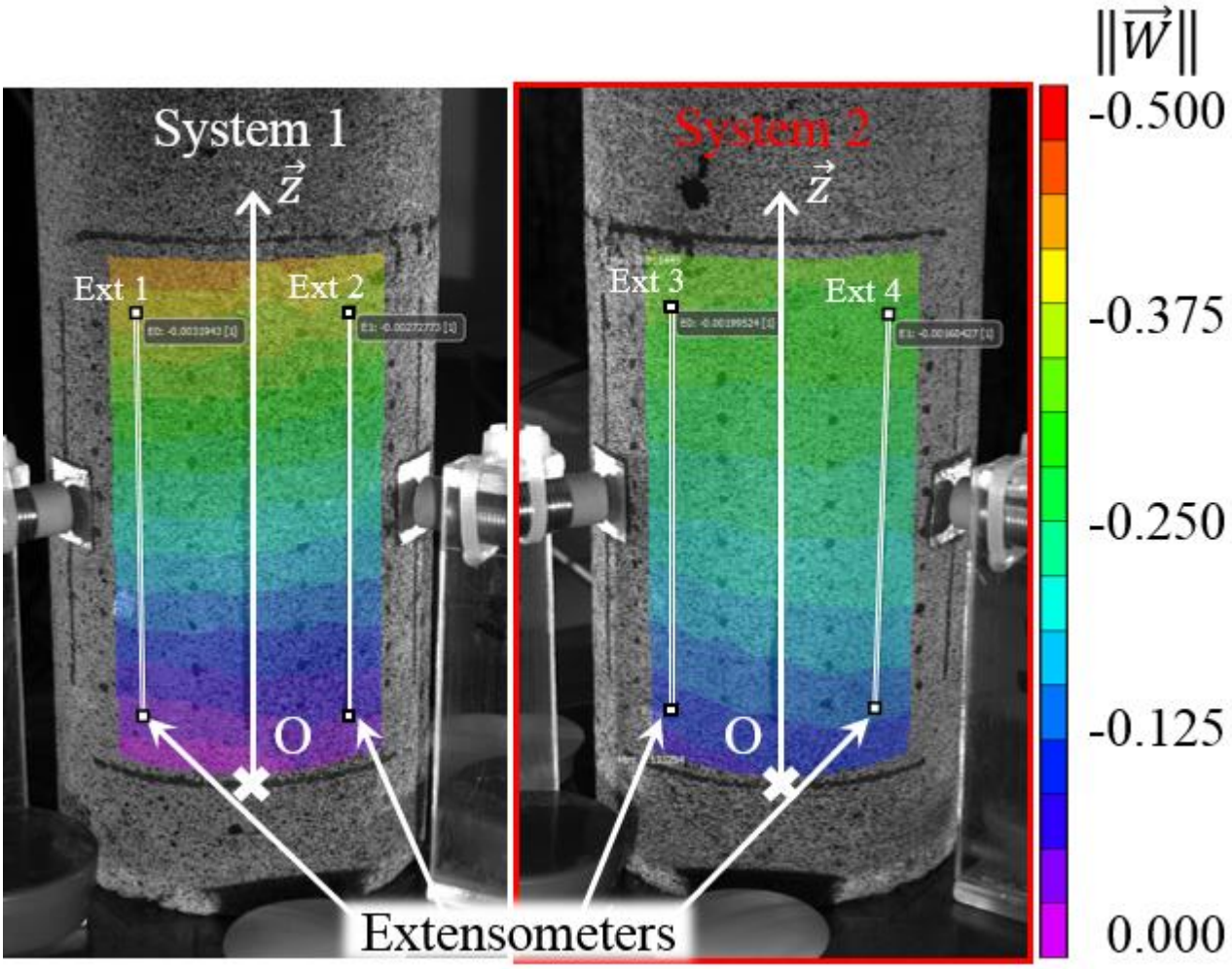

Figure 4: pictures on each camera and the correlation image for each system giving the vertical displacement field at 1MPa on STR sample equilibrated at 75%RH

A good correlation is found between the displacement fields measured by the two pairs of cameras (System 1 and System 2) since the extension of the iso-displacement lines given by the system 1 recover the iso-displacement lines given by the system 2.

To validate the ability of the image correlation device to measure with accuracy the axial strain of earth samples, the results obtained with the image correlation system were compared with the ones determined via three extensometers located in the central third of the sample during the same test. This comparison, reported in Figure 5, show a relative difference between the two devices (the values from the extensometers are the reference ones) around to 5%, which is acceptable.

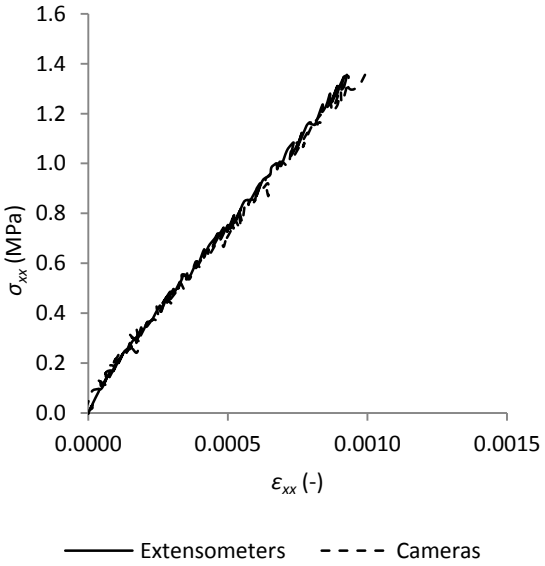

215

216 Figure 5 : Comparison between the axial strains measured by extensometers and the ones derivate from the image
217 correlation device (Cameras)

218

219 However, the accuracy of the radial displacements was not sufficient to properly derive the radial strains.
220 These latter were thus measured with three non-contact sensors (9U Kaman, Colorado Springs, USA), with a
221 resolution of 0.4 µm and a range of 4 mm. As it is shown in Figure 2, the sensors were placed at 120° around
222 the sample. The target was an aluminum pastille glued with silicone grease on the sample.

223

224 **3.4. Loading characteristics**

225 Two types of loading were made on each earth and humidity. The first loading type is a classical unconfined
226 compression test: loading at constant speed until failure. It allows measuring the compressive strength, noted
227 f_c in the following. The second loading type consists of successive unloading-reloading cycles with an
228 increasing stress level at respectively 20%, 40%, 60% and finally 80% of f_c ; where f_c is the compressive
229 strength obtained with the first loading type on the same earth and at the same humidity. The cycles were
230 implicitly assumed to have no impact on the compressive strength. In addition, the behavior of the material is
231 supposed to be linear and elastic during the cycles. These hypotheses were checked *a posteriori*. In
232 consequence, this second loading type allows determining Hooke's law elastic parameters, namely the
233 Young's modulus, E, and the Poisson's Ratio, ν, and their variations with the maximal axial stress applied on
234 the sample. These latter are then estimated through:

$$E = \frac{\Delta\sigma_{xx}^{cycle}}{\Delta\varepsilon_{xx}^{cycle}} \;;\; 1 - 2\nu = \frac{\Delta\varepsilon_{v}^{cycle}}{\Delta\varepsilon_{xx}^{cycle}} \quad (1)$$

where $\Delta\sigma_{xx}^{cycle}$, $\Delta\varepsilon_{xx}^{cycle}$ and $\Delta\varepsilon_{v}^{cycle}$ are the difference in the axial stress, the axial strain and the volumetric strain between the maximal and minimal load states of a cycle.

The loadings were controlled in displacement with a speed of 0.002mm/s in loading and unloading. This loading rate was chosen in order to make at least 200 pictures during the first unloading-reloading cycles. Before each test, a pre-loading stage up to 0.07 MPa was applied for sample mounting. It was chosen in order to be far lower than the strength of the tested material (in the range or higher than 1 MPa).

4. Results

4.1. Tests without cycles

The results of the unconfined compression tests without cycle for the STR earth samples are reported in Figure 6. The evolution of axial stress with axial strain is given in Figure 6A and the evolution of volumetric strain with axial strain in Figure 6B. Similarly, the results of CRA and ALX samples are reported in Figure 7 and Figure 8.

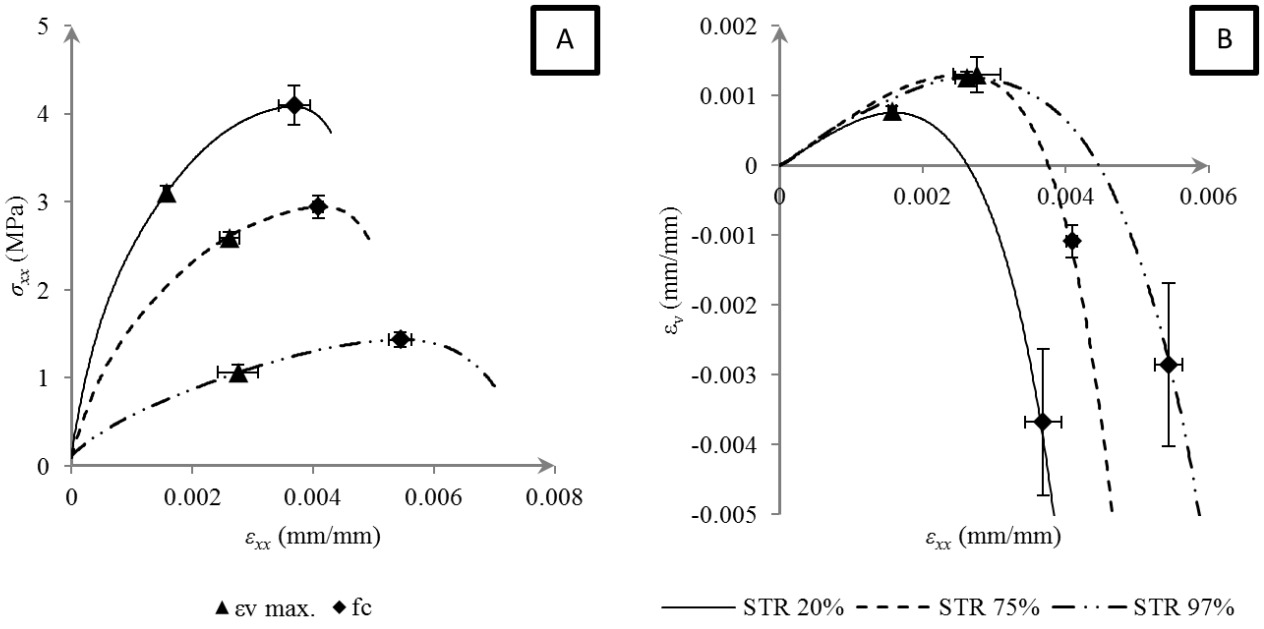

Figure 6 : Evolution of axial stress (A) and volumetric strain (B) vs axial strain for STR and their respective standard deviation calculated with 3 samples. "fc" denotes the point at which the maximum axial stress is reached while "εvmax" is the one at which the maximum axial strain is reached.

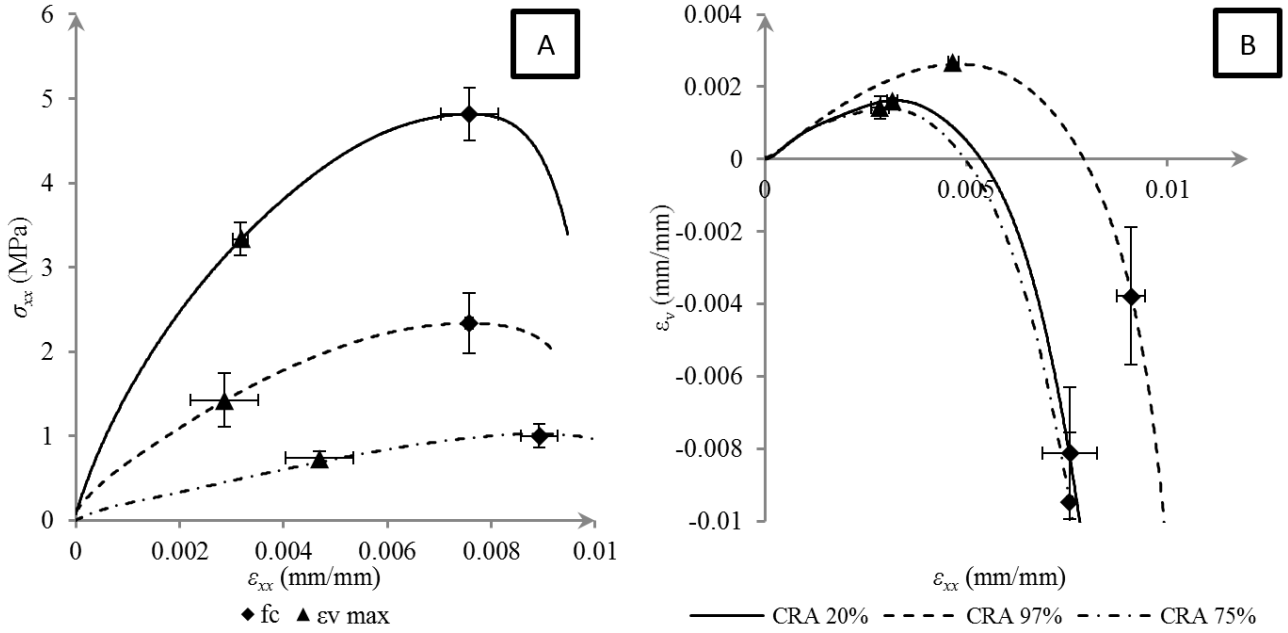

Figure 7 : Evolution of axial stress (A) and volumetric strain (B) vs axial strain for CRA and their respective standard deviation calculated with 3 samples. "fc" denotes the point at which the maximum axial stress is reached while "εvmax" is the one at which the maximum axial strain is reached.

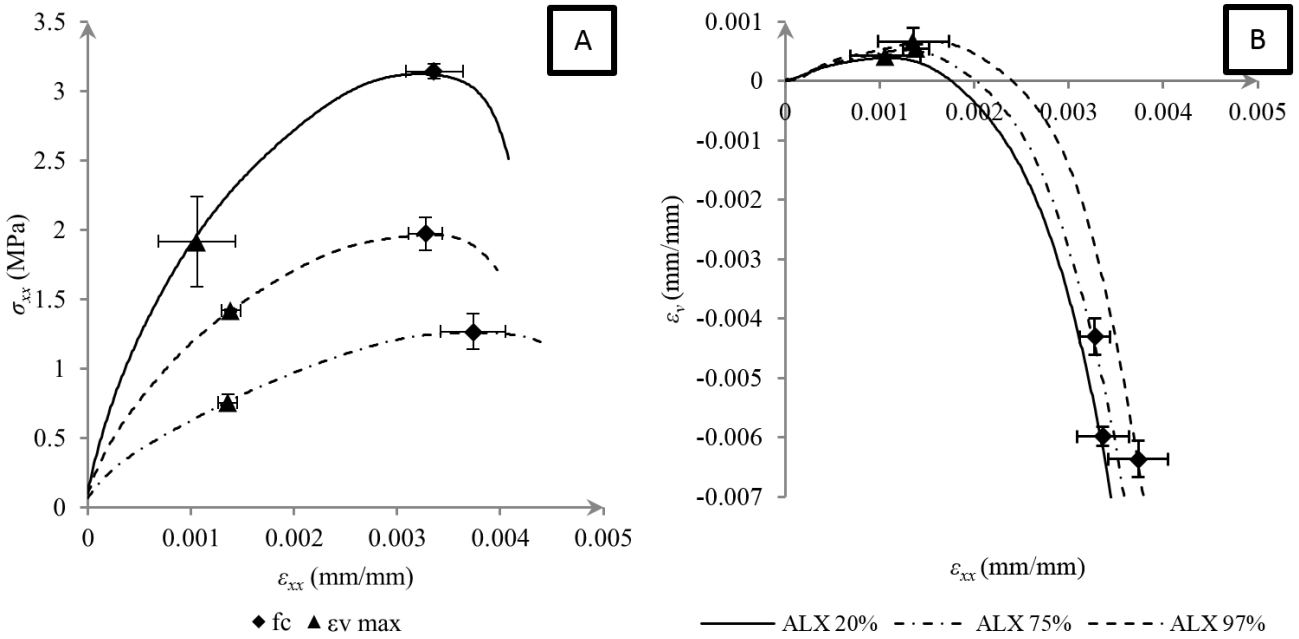

Figure 8 : Evolution of axial stress (A) and volumetric strain (B) vs axial strain for ALX and their respective standard deviation calculated with 3 samples. "fc" denotes the point at which the maximum axial stress is reached while "εvmax" is the one at which the maximum axial strain is reached.

At first, the analysis of the relationship between axial stress and axial strain (Figure 6A, Figure 7A and Figure 8A) show that the compressive strength decreases with relative humidity whatever the earth (STR, ALX or CRA). This observation is in accordance with the data already published on earthen materials (e.g. [9], [13], [32], [35], [36]).

Let us now consider the relation between volumetric and axial strains (Figure 6B, Figure 7B and Figure 8B). For low axial strains, the behavior is contractant (ε_v is positive). However, at a certain value of axial strain, the volumetric strain reaches its peak value and decreases afterwards ($\partial\varepsilon_v/\partial\varepsilon_1$ becomes negative); in other words, the behavior becomes dilatant. In particular, when the axial stress is equal to f_c, the sample has a volume higher than its initial volume (ε_v negative). This tendency is observed for all samples tested whatever the earth and the storage relative humidity.

4.2. Tests with load cycles

As mentioned before, the goal of the tests with unloading-reloading cycles was to determine the elasticity parameters (namely Young's Modulus and Poisson's ratio) and their dependence on relative humidity and maximum axial stress experienced by the sample. Consequently, it is at first necessary to verify that the materials behavior is linear elastic during the cycles. The results for STR samples at 25%RH are sketched in

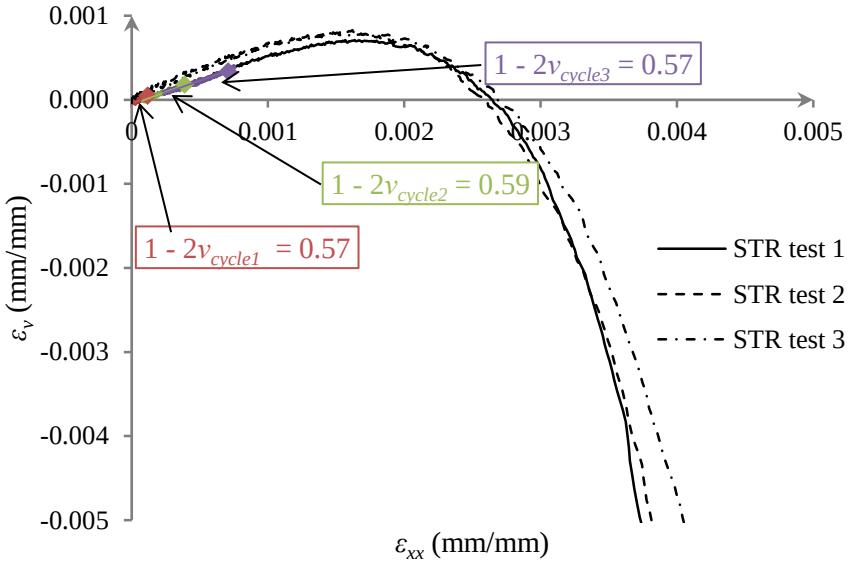

Figure 9 and results for CRA samples at 25%RH in Figure 10. The same tendency is observed for all other tested samples.

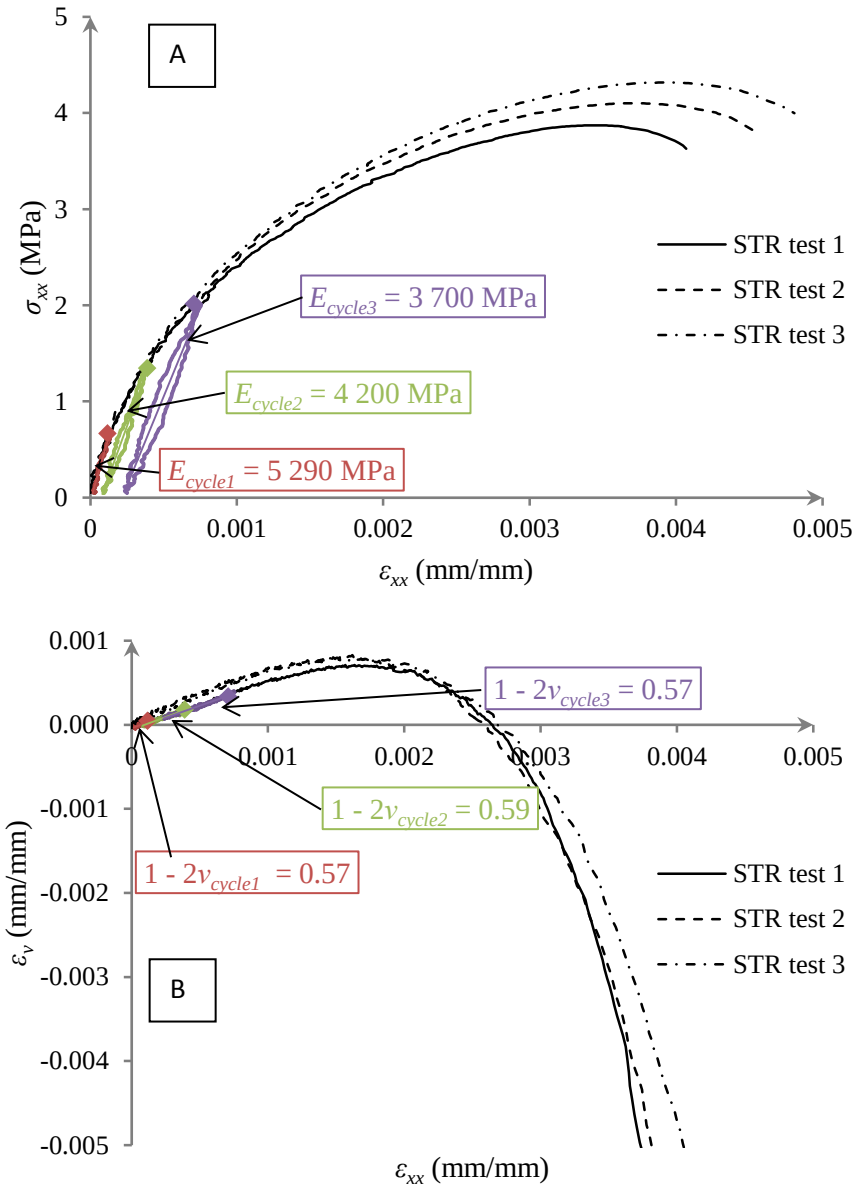

Figure 9 : Evolution of axial stress (A) and volumetric strain (B) vs axial strain during loading and unloading for the STR earth at 25% of humidity

No matter which earth is tested and the level of applied stress, the stress-strain relation is almost linear during both unloading and reloading stages (cf.

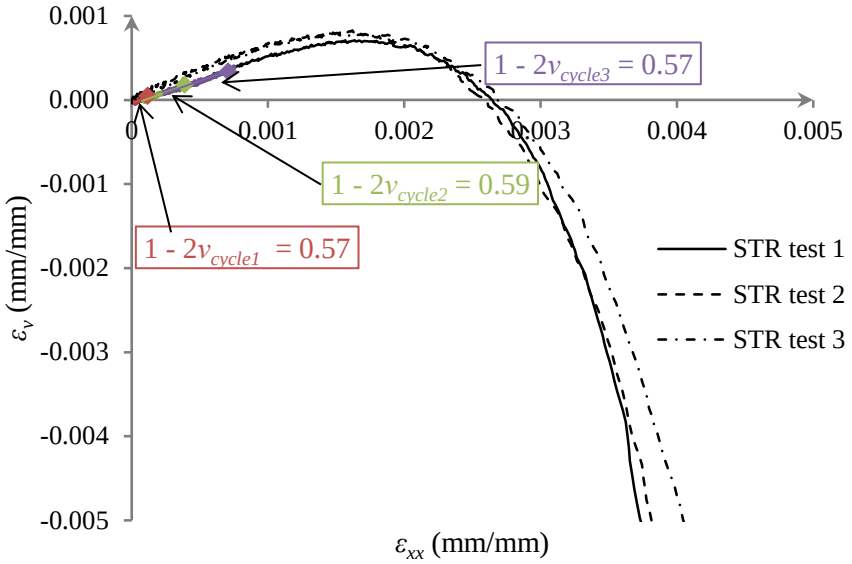

Figure 9A and Figure 10A). Small hysteresis loops can be observed, especially when the maximal axial stress increases. However, they remain limited, and the elastic linear assumption is, at first order, validated.

The analysis of the stress-strain relation during the cycle underlines that both the secant Young's modulus and the residual strain associated with each cycle depend on the nature of earth and on the conditioning relative humidity. For illustrative purpose, at the same relative humidity (25%RH) the residual axial strain after the first cycle of CRA is 40% higher than the STR one. This point is discussed more in detail in the next section.

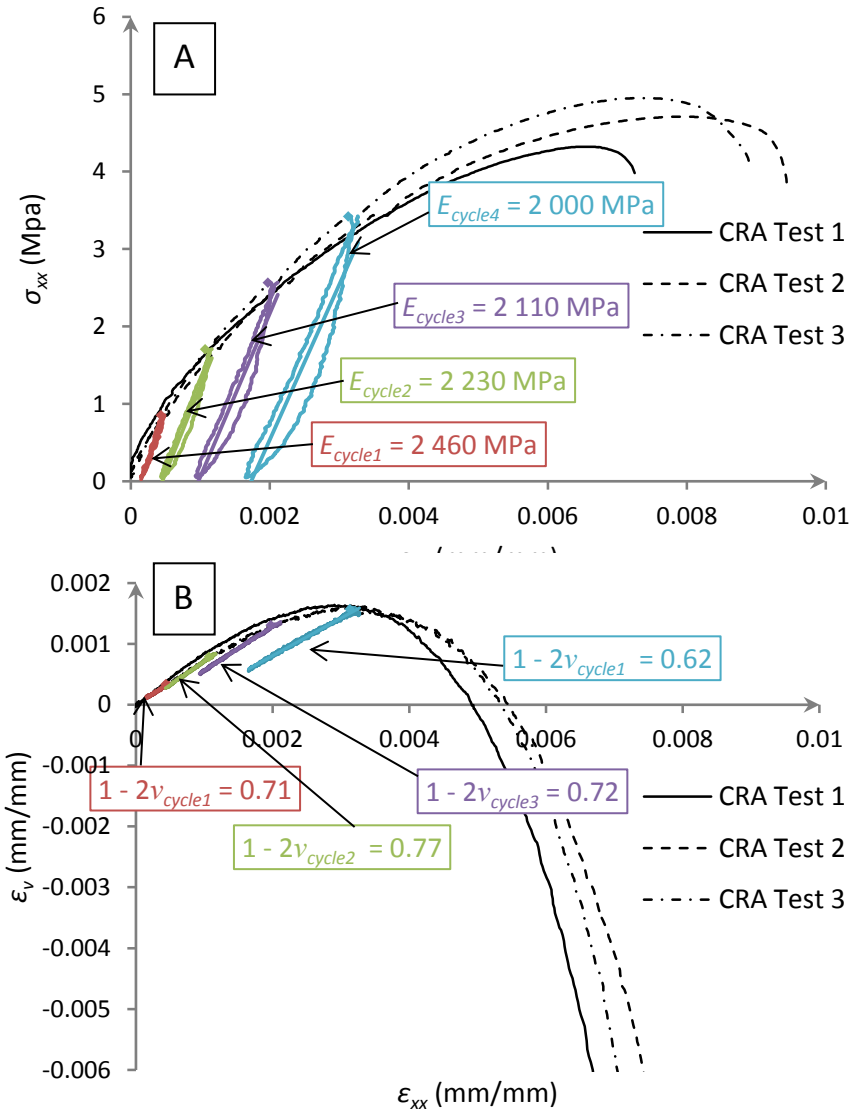

Figure 10 : Evolution of axial stress (A) and volumetric strain (B) vs axial strain during loading and unloading for the CRA earth at 25% of humidity

Now, let us focus on the volumetric behavior during the loading cycles. In

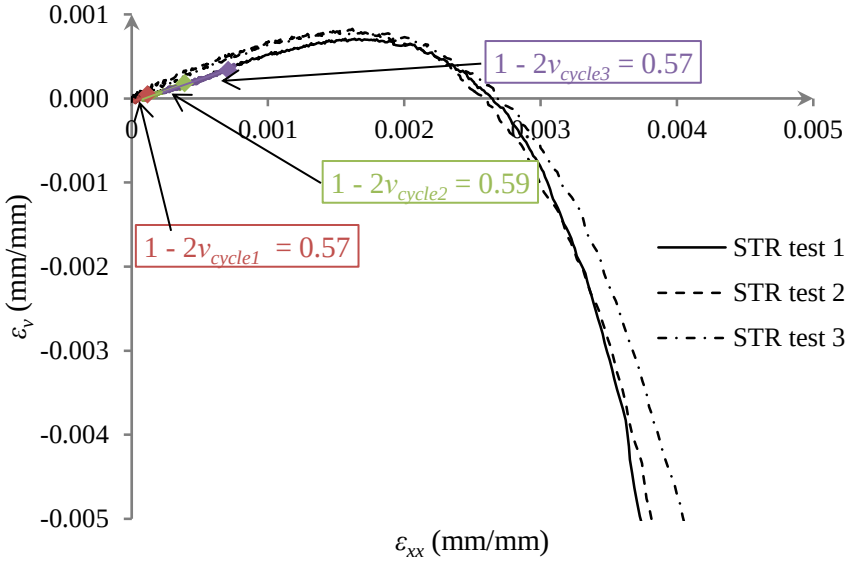

Figure 9B and Figure 10B, until the axial stress reaches 60% of f_c, the relation between volumetric and axial strains stays linear. This linearity is not modified by the loading cycles and matches with a Poisson's ratio ranging from 0.15 to 0.2. As mentioned in the previous part, when the axial stress goes beyond a threshold value (which is close to the axial strain at 60% of f_c for all the tested samples), the behavior becomes non-linear and a transition toward dilatancy is observed. Nevertheless, during the loading cycle at 80% of f_c, a linear relation between ε_v and ε_1 with a Poisson's ratio ranging from 0.15 to 0.2 is also observed. As a consequence, the hypothesis of constant Poisson's ratio seems to be confirmed on the tested materials and in the range of moisture content corresponding to HR in the range 25%-97%. On the other hand, Poisson's ratios obtained in this study are significantly lower than 0.33, which is the value used in some previous studies [12].

5. Discussion

Experimental results exposed in this study underline the influence of storage relative humidity on the behavior of the material, given that the overall mechanical behavior appears to be different for all the earthen material tested.

These differences are well illustrated by the evolution of the secant Young's modulus during a cycle of unloading-reloading against the maximum axial stress previously reached for all the tested samples, reported in upper graphs of Figure 11. The results obtained on STR and ALX samples are consistent with the study reported by [13] where a global reduction of the Young's modulus with increasing axial stress is observed.

Nonetheless, this tendency should be tempered depending on the type of earth and moisture content. Indeed, whatever the humidity and the stress level, the variation of the secant Young's Modulus of the CRA samples with the magnitude of the loading remains limited (lower than 10%). The variation of the Young's modulus with the stress level is also drastically reduced when the moisture content of the sample increases, regardless of the type of earth. For example, reduction of the Young's modulus between the first and the last cycles is around 38% for the ALX samples conditioned at 25%RH, while it is around 5% for the ones conditioned at 97%RH. As shown in Figure 11, this tendency is also observed on STR samples.

It may be interesting to compare these variations with the evolutions of the residual strains with the loading level, which are reported in the bottom graphs of Figure 11. The global tendency observed is quite obvious: when the stress level increases, the residual strain also increases. However, a close examination of these graphs shows that for a given stress level and a given earth, the residual strain tends to increase with the moisture content. In addition, at the same stress level and humidity, the residual strains of CRA samples are significantly higher than that of STR and ALX samples. For example, the residual strain after the third unload, with a conditioning humidity of 25%RH, is around 0.2 µm/m for STR and 0.4 µm/m for ALX, while that of CRA is about 1 µm/m. As shown in Figure 11, this tendency is also observed for other relative humidity.

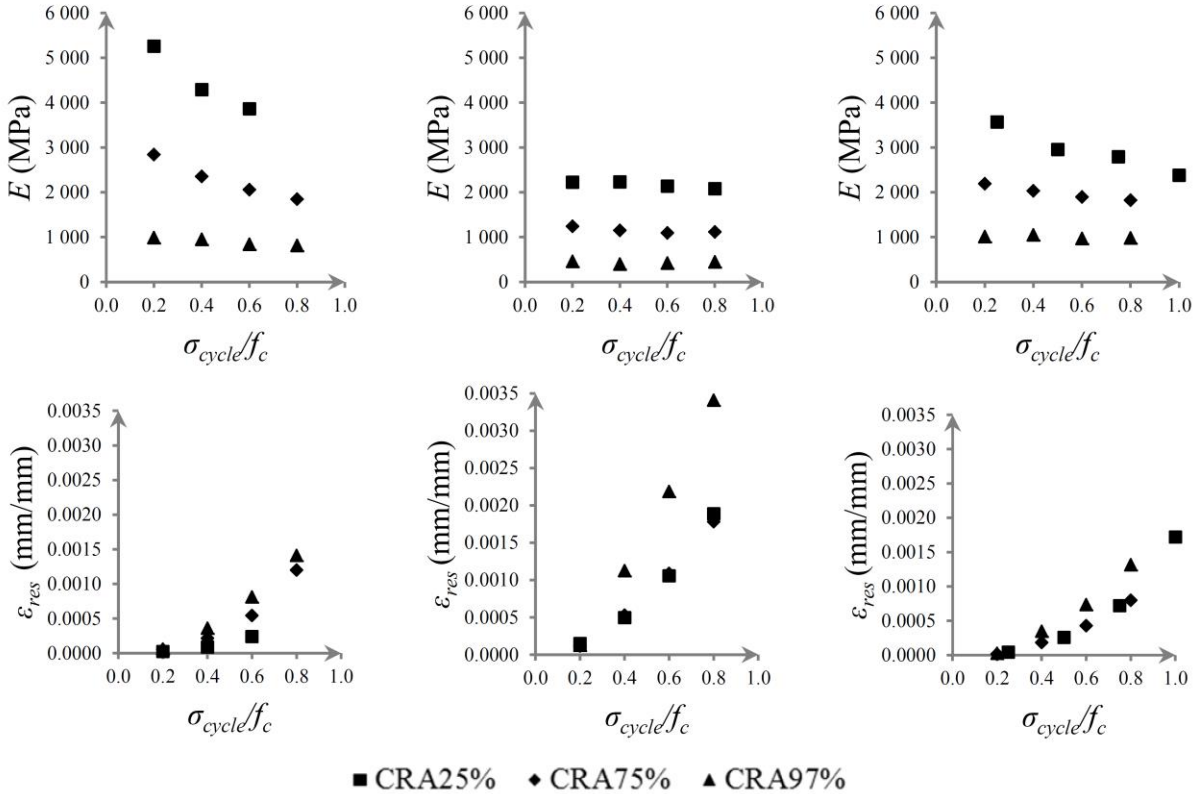

Figure 11 : Young's modulus (up) and residual strain (down) as a function of stress level. ε_{res} stands for the residual strain at the end of the unloading stage of the cycle and σ_{cycle} for the maximal axial stress of the unloading-loading cycle.

CRA samples exhibit strong irreversible strain, even at quite low loading levels, while almost no damage is observed. On the contrary, STR samples seem to be altered by damage, but show a less important plastic behavior. The clay content and, in general, the particle size distribution of these two earths is nearly the same. However, the plasticity index and the methylene blue value of CRA are at least twice as high as those of STR. At last, ALX samples, for which the plasticity index and blue value are also more than two times lower than those of CRA, show the same type of behavior as STR samples, although their particle size distribution and clay content are significantly different.

A similar discussion can be made on the relationship between the compressive strength and the Young's modulus measured during the first cycle. Indeed, as shown in Figure 12, the linear relation that seems to be shared by STR and ALX samples does not apply for CRA samples whose slope is significantly higher.

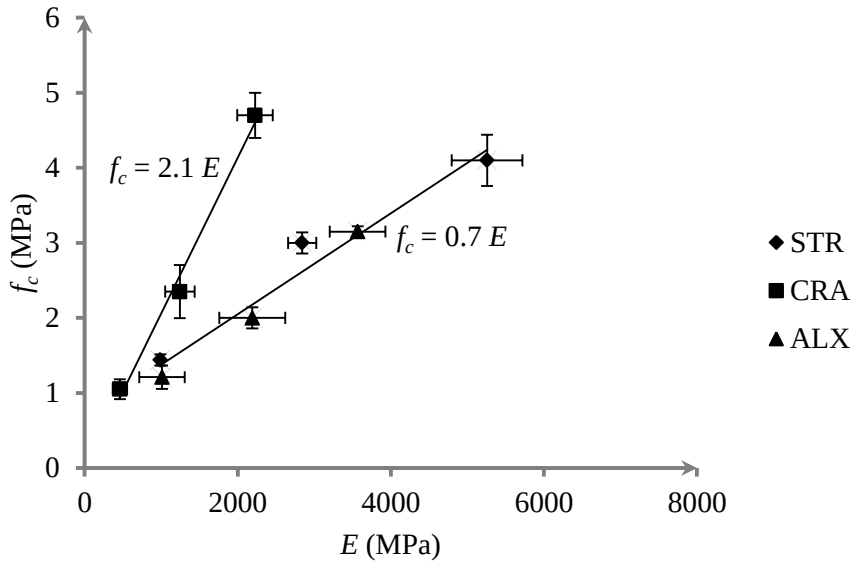

Figure 12 : Compressive strength against the Young's modulus evaluated during the first cycle

These comparisons tend to support the conclusion that the activity of the clays, qualified by methylene blue value, seems to have a more important impact on the mechanical behavior of compacted earth than the amount of clays, quantified by the particle size distribution, as long as its amount remains sufficiently important to ensure the material cohesion. This observation on the mechanical behavior can also be extended to the hydric behavior; for a given storage relative humidity, the moisture content in the CRA samples is significantly higher than those in STR and ALX samples. However, the difference in the mechanical behavior of the tested

materials cannot be solely attributed to their difference in water content. Indeed, as shown in Figure 11, although the CRA samples conditioned at 25%RH have approximatively the same water content as the STR and ALX samples conditioned at 75%RH, their behavior remains significantly different.

Let us now focus on the variation of the mechanical strength and deformability as a function of the conditioning relative humidity (and moisture content). Results obtained for each earth are summarized in Figure11A for the compressive strength and in Figure11B for the Young's modulus.

First of all, for a given earth, both the compressive strength and the Young's modulus decrease with water content. This result is not surprising and was already observed in [9], [13], [32], [35], [36]. However, the magnitude of this phenomenon is surprising. Indeed, the fall in compressive strength and Young's modulus between the samples conditioned at 25%RH and 75%rRH ranges from 25% to 50% while their moisture content varies a little (less than 0.5 % in absolute). As it is already discussed in the previous paragraph, the same tendency is observed for the residual strains. In addition, it is important to underline that the relative humidity considered in this study correspond to those commonly encountered by most of the earthen constructions during their lifetime.

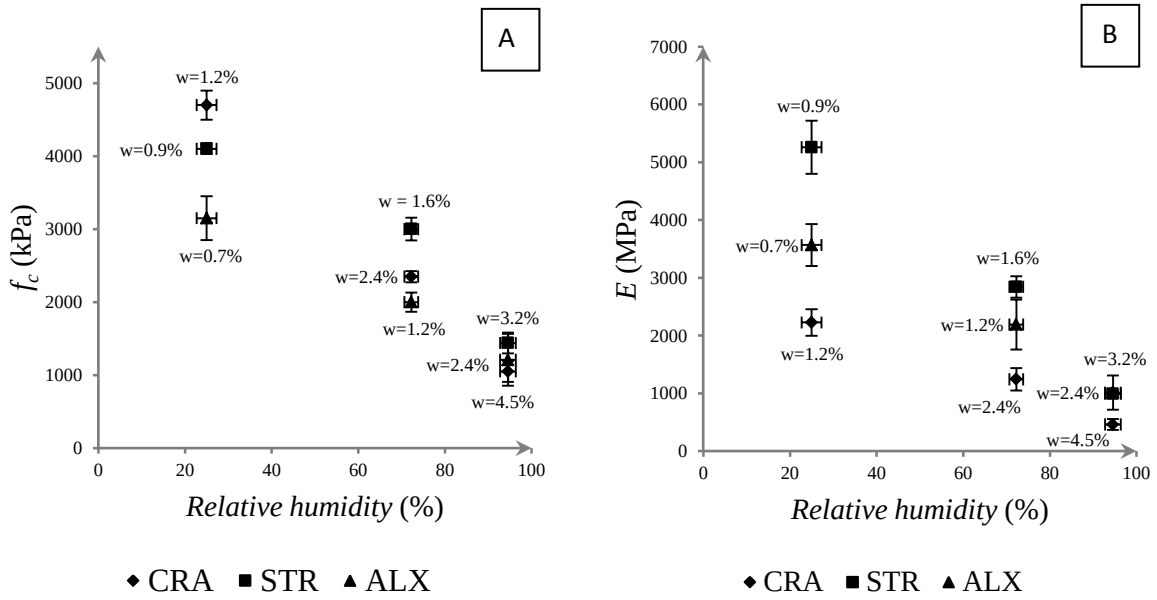

Figure 13 : Variations of compressive strength (A) and Young's modulus (B), evaluated during the first cycle (20% of f_c) against relative humidity.

To conclude, the mechanical characteristics of earth samples depend intrinsically on their water content; the test results must therefore always be interpreted accounting for this hydro-mechanical coupling. In particular,

375 the strength parameter estimation, essential for the design of an earthen building, must take into account this
376 effect, by adding, for example, a safety coefficient.

377 6. Conclusion

378 Unconfined compression tests were performed on 3 types of earth, conditioned at three relative humidity.
379 Tested samples were made out of materials coming from different existing constructions. However, the
380 particle distribution of none of them fit within the non-prescriptive recommendation suggested by [28], and
381 named BS1377-2:1990. As a consequence, the particle size distribution alone does not appear to be sufficient
382 to decide whether or not a given type of earth is suitable for rammed earth constructions.

383 Radial strains were measured with non-contact sensors. Axial strain measurements were realized by an image
384 correlation system and by the press displacement sensor. The comparison between these two axial strain
385 measurements shows the use of the displacement sensor of the press can lead to an accurate estimation of the
386 secant Young's modulus during an unload-reload cycle, as far as the press deformability is taken into account.

387 Although the tests were performed on small-size homogeneous samples without gravels, the results obtained
388 underline that earth exhibits a complex mechanical behavior which combines damage, elasto-plasticity, and
389 unsaturated mechanisms. In particular, a strong influence of the moisture content on the mechanical behavior
390 (both strength and deformability), even in the range of relative humidity commonly observed during the
391 lifetime of a building. In addition, the moisture content seems to impact the increase in plasticity
392 (characterized by the residual deformation) and damage (characterize by the drop in the Young’s modulus)
393 with the loading charge. These latter also seems to depend on the activity of the clays forming the cohesive
394 matrix of the material. However, to quantify correctly this dependency, further studies are necessary, in
395 particular aiming at lightening the impact of the clayey portion activity on the overall macroscopic mechanical
396 behavior.

397 For an exhaustive modelling of the material’s behavior, it would be necessary to use dedicated unsaturated
398 elasto-plastic damage models. The main drawbacks of this kind of models are their important number of
399 parameters, which requires numerous characterization tests to be identified. However, under normal condition
400 of use, all the complication in behavior underlined in this study may not be necessary to be considered. In
401 particular, it appears that the strength of all the tested material, whatever its water content, remains sufficiently

important (higher than 1MPa) to build load bearing walls of 50cm tick. In consequence, a next step of this study should be to identify more clearly which complexity is necessary to be taken into account as a function of the usage conditions of the material and to develop the simplified relevant theoretical law of behaviors.

7. Acknowledgement

The authors wish to thank the French national research agency ANR (PRIMATERRE – ANR-12-VBDU-0001-01 Villes et Bâtiments durables) for the funding of this project.

8. Bibliography

[1] J. C. Morel, A. Mesbah, M. Oggero, and P. Walker, "Building houses with local materials : means to drastically reduce the environmental impact of construction," *Building and Environment*, vol. 36, pp. 1119–1126, 2001.

[2] P. Chabriac, A. Fabbri, J. Morel, J. Laurent, and J. Blanc-Gonnet, "A Procedure to Measure the in-Situ Hygrothermal Behavior of Earth Walls," *Materials*, pp. 3002–3020, 2014.

[3] L. Soudani, A. Fabbri, J. Morel, M. Woloszyn, and A. Grillet, "A coupled hygrothermal model for earthen materials," *in revision in Energy and Buildings*, 2015.

[4] S. Dubois, F. McGregor, A. Evrard, A. Heath, and F. Lebeau, "An inverse modelling approach to estimate the hygric parameters of clay-based masonry during a Moisture Buffer Value test," *Building and Environment*, vol. 81, pp. 192–203, Nov. 2014.

[5] F. McGregor, A. Heath, A. Shea, and M. Lawrence, "The moisture buffering capacity of unfired clay masonry," *Building and Environment*, vol. 82, pp. 599–607, Dec. 2014.

[6] Q.-B. Bui and J.-C. Morel, "Assessing the anisotropy of rammed earth," *Construction and Building Materials*, vol. 23, no. 9, pp. 3005–3011, 2009.

[7] M. Hall and Y. Djerbib, "Rammed earth sample production: context, recommendations and consistency," *Construction and Building Materials*, vol. 18, no. 4, pp. 281–286, 2004.

[8] A. Heath, P. Walker, C. Fourie, and M. Lawrence, "Compressive strength of extruded unfired clay masonry units," *Proceedings of the ICE - Construction Materials*, vol. 162, no. 3, pp. 105 – 112, 2009.

[9] H. Nowamooz and C. Chazallon, "Finite element modelling of a rammed earth wall," *Construction and Building Materials*, vol. 25, no. 4, pp. 2112–2121, Apr. 2011.

[10] T.-T. Bui, Q.-B. Bui, A. Limam, and S. Maximilien, "Failure of rammed earth walls: From observations to quantifications," *Construction and Building Materials*, vol. 51, pp. 295–302, 2014.

[11] P. Jaquin, "Analysis of Historic Rammed Earth Construction," Dissertation, Durham University, 2008.

[12] D. Ciancio and J. Gibbings, "Experimental investigation on the compressive strength of cored and molded cement-stabilized rammed earth samples," *Construction and Building Materials*, vol. 28, no. 1, pp. 294–304, 2012.

[13] Q.-B. Bui, J.-C. Morel, S. Hans, and P. Walker, “Effect of moisture content on the mechanical characteristics of rammed earth,” *Construction and Building Materials*, vol. 54, pp. 163–169, 2014.

[14] J. C. Morel and A. Pkla, “A model to measure compressive strength of compressed earth blocks with the ‘3 points bending test,’” *Construction and Building Materials*, vol. 16, no. 5, pp. 303–310, 2002.

[15] J. E. Aubert, A. Fabbri, J. C. Morel, and P. Maillard, “An earth block with a compressive strength higher than 45 MPa !,” *Construction and Building Materials*, vol. 47, pp. 366–369, 2013.

[16] M. R. Hall, R. Lindsay, and M. Krayenhoff, *Modern earth buildings*. London: Woodhead, 2012.

[17] H. Van Damme, *Colloidal chemo-mechanics of cement hydrates and smectite clays : Cohesion vs Swelling*. London: Taylor & Francis Group, 2006.

[18] X. Lei, H. Wong, A. Fabbri, A. Limam, and Y. M. Cheng, “A thermo-chemo-electro-mechanical framework of unsaturated expansive clays,” *Computer and Geotechnics*, vol. 62, pp. 175–192, 2014.

[19] A. Hakimi, N. Yamani, and H. Ouissi, “Rapport : Résultats d’essais de résistance mécanique sur échantillon de terre comprimée,” *Materials and Structures*, vol. 29, no. December, pp. 600–608, 1996.

[20] B. Venkatarama Reddy and P. Prasanna Kumar, “Structural Behavior of Story-High Cement-Stabilized Rammed-Earth Walls under Compression,” *Journal of Materials in Civil Engineering*, vol. 23, no. 3, pp. 240–247, 2011.

[21] P. J. Walker, “Strength , Durability and Shrinkage Characteristics of Cement Stabilised Soil Blocks,” *Cement & Concrete Composites*, vol. 17, no. 95, pp. 301–310, 1995.

[22] D. Maskell, A. Heath, and P. Walker, “Inorganic stabilisation methods for extruded earth masonry units,” *Construction and Building Materials*, vol. 71, pp. 602–609, Nov. 2014.

[23] D. Ciancio, C. T. S. Beckett, and J. a. H. Carraro, “Optimum lime content identification for lime-stabilised rammed earth,” *Construction and Building Materials*, vol. 53, pp. 59–65, Feb. 2014.

[24] D. Maskell, A. Heath, and P. Walker, “Comparing the environmental impact of stabilisers for unfired earth construction,” *Key Engineering Materials*, vol. 600, pp. 132–143, 2014.

[25] B. V. Venkatarama Reddy and M. S. Latha, “Retrieving clay minerals from stabilised soil compacts,” *Applied Clay Science*, vol. 101, pp. 362–368, Nov. 2014.

[26] M. I. Gomes, T. D. Gonçalves, and P. Faria, “Unstabilized Rammed Earth: Characterization of Material Collected from Old Constructions in South Portugal and Comparison to Normative Requirements,” *International Journal of Architectural Heritage: Conservation*, vol. 8, no. 2, pp. 185–212, 2014.

[27] D. Lautrin, “Une procédure rapide d’identification des argiles,” *Bulletin de liason du Laboratoire Pont et Chaussée*, vol. 152, pp. 75–84, 1987.

[28] H. Houben and H. Guillaud, *Earth Construction: A Comprehensive Guide (Earth Construction)*. London: Intermediate Technology Publications, 1994.

[29] J.-E. Aubert, A. Marcom, P. Oliva, and P. Segui, “Chequered earth construction in south-western France,” *Journal of Cultural Heritage*, p. 6, 2014.

[30] W. F. Woodruff and a. Revil, “CEC-normalized clay-water sorption isotherm,” *Water Resources Research*, vol. 47, no. 11, p. n/a–n/a, 2011.

[31] J. C. Morel, A. Mesbah, H. Houben, and V. Rigassi, *Compressed earth blocks, testing procedures*. Belgium: ARSO, 2000.

[32] M. Olivier, “Le matériau terre, compactage, comportement, application aux structures en blocs de terre,” Dissertation, ENTPE, Université de Lyon, 1994.

[33] K. Krefeld, “Effect of shape of specimen on the apparent compressive strength of brick masonry,” *Philadelphia, USA: Proceedings of the American Society of Materials*, 1938.

[34] H. W. Schreier, M. A. Sutton, and J.-J. Orteu, *Image Correlation for Shape, Motion and Deformation Measurements*. New-York: Springer Science+Business Media, 2009.

[35] L. Miccoli, U. Müller, and P. Fontana, “Mechanical behaviour of earthen materials : A comparison between earth block masonry , rammed earth and cob,” *Construction and Building Materials*, vol. 61, pp. 327–339, 2014.

[36] P. Jaquin, D. G. Toll, D. Gallipoli, and C. E. Augarde, “The strength of unstabilised rammed earth materials,” *Géotechnique*, vol. 59, no. 5, pp. 487–490, Jan. 2009.